A Fast ECT Measurement Method for the Thickness of Metallic Plates

Alessandro Sardellitti, *Graduate Student Member, IEEE*, Giulia Di Capua, *Senior Member, IEEE*, Marco Laracca, *Member, IEEE*, Antonello Tamburrino, *Senior Member, IEEE*, Salvatore Ventre, *Senior Member, IEEE*, and Luigi Ferrigno, *Senior Member, IEEE*

***Abstract*— This contribution focuses on the nondestructive evaluation of the thickness of metallic plates, by means of eddy-current testing. Specifically, we present a method for reducing/optimizing the measurement time for the approach presented in (Yin and Peyton, 2007), while keeping a high accuracy suitable for industrial applications. In (Yin and Peyton, 2007), the key feature for estimating the thickness of plates is the value of the frequency where a proper quantity achieves its minimum value. To get a proper accuracy in measuring the thickness of the plate, this minimum needs to be located in an accurate manner. In turns, this requires "many" measurements at different frequencies, which make the approach time-consuming and not suitable for almost real-time applications, as those of interest for industry. The proposed patent pending strategy combines a multisine approach to collect the data onto a proper set of frequencies, plus proper techniques for interpolating the data at all the frequencies required to locate accurately the minimum of the response. The combination of the multisine to allocate efficiently the measurement frequencies with the data interpolation results in a reduction of the number of required measurements and, in ultimate analysis, of the overall measurement time. Specifically, the measurement time for a typical situation was reduced of a factor of about 4 (from 13 to 2.66 s) with the same accuracy level of the order of 3%. Finally, we highlight that both design and testing of the new measurement method were carried out by combining numerical simulations and experimental results.**

***Index Terms*— Eddy-current testing (ECT), nondestructive evaluation (NDE), nondestructive testing (NDT), thickness measurement.**

I. Introduction

THICKNESS measurements play a very important role in many industrial applications related to metallic laminates. Indeed, they provide information about the quality of the production, the capability of crash energy absorption, the safety of parts. These aspects are crucial in application fields such as automotive and aerospace, where the integrity of the metal laminates has a direct impact on the safety of human beings.

To warrant a zero defect production with acceptable costs and inspection time, as requested by the Industry 4.0 paradigm, three aspects are of paramount importance: 1) quality control should be executed directly during the production phase of each element; 2) automated methods able to warrant high repeatability and reproducibility of the results, together with low inspection times, should be adopted; and 3) measurement accuracies have to be compatible with those required by specific application standards such as, for instance, those related to the production of cold rolled aluminum sheets [1].

In the actual industrial practice, some metrological checks are carried out by using touch-trigger probes. Unfortunately, such measurements are time-consuming and not suitable for the integration within the production processes [2]. Other options are laser and ultrasound methods. Concerning laser-based measurement methods, we highlight that they allow *in situ* measurements with very good measurement accuracies [3], but the higher cost of the equipment has a major impact on the overall product cost. Concerning ultrasound methods, they represent a possible alternative to optical methods, as far as the measurement accuracy are concerned, but they usually require the coupling gel that imposes expensive procedure for cleaning the specimen, the use of expensive measurement systems [4]–[6], and the presence of qualified technicians to perform the test. All these aspects make this kind of tests not suitable for the inline thickness monitoring during the manufacturing stage.

Thickness measurement methods based on eddy-current testing (ECT) can be usefully used in all those applications in which it is important to measure the thickness of metal plates (e.g., automotive, aerospace, etc.). These methods can be an excellent solution to this purpose thanks to: 1) the high accuracies; 2) the high repeatability and sensitivity; 3) the possibility to automatize the test; 4) the immunity to nonconductive materials present on the specimen (e.g., dust, painting, insulating cover); 5) the possibility to carry out measurements without physical contact with the specimen; and 6) the cheapness of the probe [7]. To this aim, in [8]–[10], Yin *et al.* proposed and optimized measurement probes and processing algorithms developed *ad hoc* for the measurement

Manuscript received 21 February 2022; revised 9 May 2022; accepted 10 June 2022. Date of publication 13 July 2022; date of current version 21 July 2022. The work was supported in part by the University of Cassino and Southern Lazio through the project "Sistemi distribuiti intelligenti," funded by the MIUR Italian Ministry of University and Research, under the program "Dipartimenti di Eccellenza 2018-2022." The Associate Editor coordinating the review process was Dr. Boby George. *(Corresponding author: Marco Laracca.)*

Alessandro Sardellitti, Giulia Di Capua, Antonello Tamburrino, Salvatore Ventre, and Luigi Ferrigno are with the Department of Electrical and Information Engineering, University of Cassino and Southern Lazio, 03043 Cassino, Italy.

Marco Laracca is with the Department of Astronautics, Electrical and Energy Engineering, University of Rome "La Sapienza," 00185 Rome, Italy (e-mail: marco.laracca@uniroma1.it).

Digital Object Identifier 10.1109/TIM.2022.3188029

of the thickness of nonmagnetic materials by means of ECT. Specifically, their method gives an accuracy compatible with industrial production standards and proper immunity to lift-off variations. In detail, thanks to the Dodd and Deeds model [11], they were able to relate the thickness of a planar (and infinite slab) to the frequency where the minimum of a proper quantity is achieved. They proved experimentally the effectiveness of the method [8]–[10], showing that it exhibits very good accuracies in-line with those required for industrial manufacturing [1]. However, to warrant the desired measurement accuracies, the method proposed by Yin *et al.* requires measurements with very narrow frequency resolutions. This is a major issue when the nominal width of the specimen under test is unknown, because the method requires the exploration of a large frequency range (few hertz to some kilohertz) with a very narrow frequency resolution. These two aspects lead to an increase of the measurement time that might reach tens of seconds or more, making it not suitable for inline industrial applications.

With the aim of minimizing the overall measurement time but keeping the required measurement accuracy, this article proposes several optimizations of the measurement method described in [8]. In detail, the optimizations are carried out along two main routes: a) the use of smart excitation strategies able to minimize the measurement time and b) the use of improved processing algorithms able to warrant the desired accuracy even in presence of a minimal set of measured signals. In detail, regarding a) a dual-stage measurement procedure based on optimized multifrequency signals has been implemented to reduce the measurement time [12], [13]. Concerning b) proper interpolations have been implemented to achieve the required measurement accuracies. A huge experimental campaign confirmed that the proposed optimized measurement method minimizes the overall measurement time while keeping the required measurement accuracy.

This article is organized as follows. In Section II, the theoretical background with an analysis and a critical discussion on the limits of the measurement time for the actual solutions is reported. In Section III, the proposed method to improve the measurement solution analyzed in Section II is described: multifrequency signals in Section III-A and interpolating techniques in Section III-B. The experimental setup and the case study under investigation are reported in Section IV. The simulation and experimental results are reported and discussed in Sections V and VI, respectively. The results show that the proposed ECT-based measurement method allows to measure the thickness with an accuracy in line with that required by the standards in industry, while keeping the measurement time suitable for almost real-time applications.

II. Theoretical Background and Rationale of the Article

The typical basic operating principle of ECT is as follows: an excitation coil induces eddy currents in the test sample, while magnetic sensors or sensing coils measure the reaction magnetic flux density [14]. The analysis of the reaction flux density allows to define the characteristics of the investigated material.

The thickness measurement solution proposed in this manuscript is derived from swept frequency (SF) methods [8]–[10], [15], [16]. Other available approaches are based on pulsed ECT (PECT) methods [17]–[20]. PECT methods achieve their best performances when the thickness to be measured is estimated via a proper feature from time domain data. As a matter of fact, PECT signals can be used to get swept-frequency data but may result to be not optimal. Indeed, the harmonic content of the applied signal decay fast with the order of the harmonic itself. For instances, in the case of the widely used rectangular pulse, the energy of the harmonics decays as $1/n^2$, with impact on the signal-to-noise ratio. Another potential issue is that the tones of PECT signals are allocated at frequencies which are multiple of the inverse of the fundamental period of the (periodic) waveform. This specific distribution of the tones may be not optimal for a specific application as the present one. Our approach is somehow in an intermediate position between SF and PECT: we avoid a direct swept-frequency approach by selecting a proper set of discrete frequencies of interest and we use a multisine strategy to allocate the energy of the signal in a controlled manner. Interpolation techniques are used to extract the relevant frequency domain feature from the measured data.

The following subsections are devoted to explain the theoretical background of the analytical model used in [8]–[10] and the analysis of the measurement time and accuracy performances of the method.

A. Description of the Reference Analytical Model

Analytical solutions for axially symmetric eddy-current problems have been proposed and discussed in the literature. Specifically, in a well-known paper by Dodd and Deeds [11], it is given a mathematical model for the eddy-current computation for a coil above a single or multiple planar (infinite) conductive plates of finite thickness and different electrical conductivity. Starting from this semi-analytical model, Yin *et al.* proposed different probes, methods, and processing algorithms, suitably developed for estimating the thickness of nonmagnetic materials. The proposed solutions are able to obtain thickness measurement accuracies compatible with industrial production standards and low sensitivity to lift-off variations [9], [10].

Without loss of generality, in this article, the attention was focused on the double coaxial coil proposed in [9]. In particular, it was considered a measuring system involving the use of two coils: one driving coil and one pick-up coil. Given the geometry shown in Fig. 1, it is possible to calculate the mutual impedance between the two coils when they are placed onto the specimen ($\dot{Z}_{m,\text{plate}}$) or in the air ($\dot{Z}_{m,\text{air}}$), by the Dodd and Deeds model. Specifically, $\dot{Z}_{m,\text{plate}}$ and $\dot{Z}_{m,\text{air}}$ are given in the following equations:

$$\dot{Z}_{m,\text{plate}} = K \int_0^\infty L\left[C\left(F + \frac{EN}{D}\right)\right] d\alpha \tag{1}$$

$$\dot{Z}_{m,\text{air}} = K \int_0^\infty LCF\, d\alpha \tag{2}$$

where

$$K = \frac{j\omega\pi\mu_0 N_1 N_2}{(l_{22} - l_{12})(l_{21} - l_{11})(r_{21} - r_{11})(r_{22} - r_{12})} \tag{3}$$

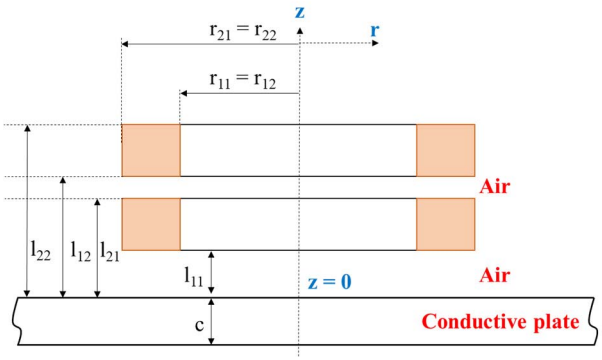

Fig. 1. Representation of the axis-symmetrical coils placed on the plate.

$$L = \frac{I(r_{11}, r_{21}) \cdot I(r_{12}, r_{22})}{\alpha^6} \tag{4}$$

$$C = e^{-\alpha l_{12}} - e^{-\alpha l_{22}} \tag{5}$$

$$F = e^{\alpha l_{21}} - e^{\alpha l_{11}} \tag{6}$$

$$E = -\left(e^{-\alpha l_{21}} - e^{-\alpha l_{11}}\right) \tag{7}$$

$$N = (\alpha\mu_R + \alpha_1)(\alpha_1 - \alpha\mu_R) + (\alpha\mu_R - \alpha_1)(\alpha_1 + \alpha\mu_R)e^{2\alpha_1 c} \tag{8}$$

$$D = (\alpha\mu_R - \alpha_1)(\alpha_1 - \alpha\mu_R) + (\alpha\mu_R + \alpha_1)(\alpha_1 + \alpha\mu_R)e^{2\alpha_1 c} \tag{9}$$

$$\alpha_1 = \sqrt{\alpha^2 + j\omega\sigma\mu_0}. \tag{10}$$

N_1 and N_2 are the number of windings of the lower coil and the upper coil, respectively, $\omega = 2\pi f$ is the angular frequency being f the frequency of the excitation signal, σ is the electrical conductivity of the material, μ_0 is the magnetic permeability of the vacuum, μ_R is the relative magnetic permeability of the material, α is the spatial frequency, and c is the thickness of the sample. All the relevant geometrical parameters $l_{11}, l_{12}, l_{21}, l_{22}, r_{11}, r_{12}, r_{21}$, and r_{22} are described in Fig. 1. Starting from these formulas, Yin *et al.* related the thickness of a planar sample to a proper frequency. Specifically, in [8] and [9], they proposed to identify the thickness of the specimen by considering the real part of the variation of either the self-impedance or the mutual impedance due to the presence of the specimen, divided by the angular frequency $2\pi f$, i.e., by considering

$$\frac{\Delta R}{\omega} = Re\left(-\frac{\dot{Z}_{m,\text{plate}}(f) - \dot{Z}_{m,\text{air}}(f)}{\omega}\right). \tag{11}$$

The thickness c of the sample is related to the frequency $f_{\min}$ where $\Delta R/2\pi f$ achieves its minimum (see Fig. 2), hereafter referred to as the "peak frequency." Specifically, the thickness can be evaluated as discussed in [9], namely:

$$c = \frac{\alpha_0}{\sigma\mu_0\pi f_{\min}} \tag{12}$$

where α_0 is the "characteristic spatial frequency" related to the system. The quantity α_0 can be evaluated numerically or experimentally.

In Section II-B, an analysis of both the measurement time and the accuracy that can be achieved is reported. In particular, we focus on the measurement time and accuracy for estimating

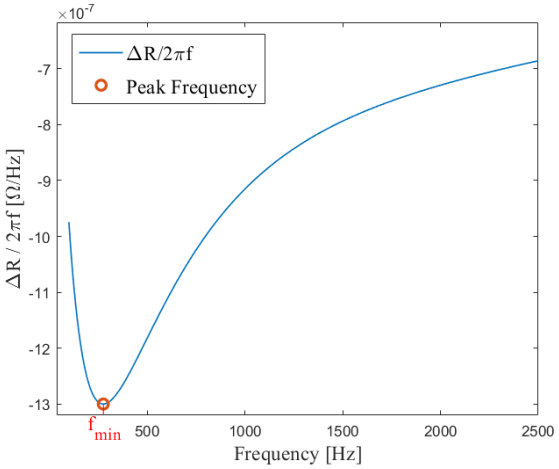

Fig. 2. Example for the $\Delta R/2\pi f$ ratio.

TABLE I
PERCENTAGE THICKNESS ESTIMATION ERROR OBTAINED IN [8]

Type of probe	Material	Actual Thickness [mm]	Relative Error [%]
Air-cored Coil	Copper	0.022	0.40
		0.044	2.50
		0.066	1.89
		0.088	2.75
		0.110	-1.65
		0.132	-2.61
U-cored coil	Aluminum	1.000	-0.37
		2.000	-0.53
		3.000	-1.48
		4.000	0.59
		5.000	1.41

the key parameter of appearing in (12), i.e., $f_{\min}$. This analysis is carried out in view of a possible online and general-purpose application of this method.

B. Analysis of Measurement Time

The measurement time, for a prescribed accuracy, represents a major limitation in the industrial scenario. Reasonable times to carry out a thickness measurement can be in the order of few seconds. However, when the unknown thickness varies in an "extended" range, it can be necessary to perform a large frequency scan.

A measurement method based on swept-sine signal turn out to be time-consuming. Moreover, the typical measurement accuracy prescribed by standards [1] calls for a frequency scan with a proper "small" step Δf, requiring the use of a high number of tones to scan a large frequency range. In [8], measurement results for copper and aluminum plates with constant lift-off value and different types of probes are discussed. The accuracy provided by these measurements is in the range of $\pm 3\%$, as shown in Table I.

To evaluate the larger value for Δf which provides the prescribed metrological performances of [8], we performed a parametric analysis. It was assumed a frequency range from 100 to 5000 Hz with a frequency resolution of 5 Hz.

TABLE II

ANALYSIS OF THE PERCENTAGE THICKNESS ESTIMATION ERROR (e_c) FOR DIFFERENT VALUES OF THE FREQUENCY RESOLUTION Δf CONSIDERING A FREQUENCY RANGE FROM 100 Hz TO 5 kHz

		Actual Thickness [mm]				
		0.1	0.2	0.3	0.4	0.5
Δf [Hz]	2	±0.02%	±0.04%	±0.06%	±0.09%	±0.11%
	5	±0.06%	±0.11%	±0.17%	±0.22%	±0.27%
	10	±0.12%	±0.22%	±0.33%	±0.44%	±0.55%
		Actual Thickness [mm]				
		1	2	3	4	5
Δf [Hz]	2	± 0.11%	±0.22%	± 0.31%	±0.39%	±0.46%
	5	±0.28%	±0.54%	± 0.78%	±0.98%	±1.14%
	10	±0.56%	±1.08%	±1.54%	±1.94%	±2.26%

This frequency range is suitable for samples with thicknesses ranging from 0.35 to 6 mm (at σ equal to 18 MS/m), or samples with thicknesses ranging from 0.1 to 5 mm (at σ equal to 59 MS/m), as one can find by means of the semi-analytical model by Dood and Deeds described in Section II-A. The thickness estimation error in the following analysis was evaluated by only taking into account the contribution due to effect of Δf in the estimation of the peak frequency $f_{\min}$, and considering negligible all the other effects (e.g., measurement setup and noise on the measured signals in the evaluation of $\Delta R/\omega$, and so on). Table II shows the percentage thickness estimation error (e_c) versus the frequency resolution, for ten different thickness values.

The e_c values have been estimated as detailed in the following.

1) Given the actual thickness (c_{ac}) and the electrical conductivity (specifically 58.7 MS/m, typical electrical conductivity of copper, has been used), the peak frequency ($f_{\text{min\_ac}}$) can be estimated by using the semi-analytical model and the geometrical system described in Section II-A (11).
2) Given the peak frequency $f_{\text{min\_ac}}$, the new values f_{min1} and f_{min2} are evaluated by subtracting/adding the value of the considered frequency resolution ($f_{\text{min1}} = f_{\text{min\_ac}} - \Delta f$ and $f_{\text{min2}} = f_{\text{min\_ac}} + \Delta f$).
3) Using (12), the new thickness values $c_{\min}(f_{\text{min2}})$ and $c_{\max}(f_{\text{min1}})$ are estimated.
4) The percentage thickness estimation errors are evaluated as: $e_c = \pm{}^1\!/_2(c_{\max} - c_{\min})/c_{\min} \cdot 100$.

As confirmed by Table II, the estimation error increases with the frequency resolution Δf and the thickness c. Performances similar to those of Table I can be achieved by using a frequency resolution less than 5 Hz.

In view of practical applications, it is relevant to analyze the time required to carry out the whole measurement process. The analysis is made by considering two measurement solutions: 1) the impedance analyzer used in [8] to obtain the performances shown in Table I (similar results can be obtained considering other impedance analyzers) and 2) a general-purpose device to be able to generate the excitation signal and to acquire the desired quantities. Obviously, the accuracy performance in the thickness measurement depends on the characteristics of the used device and on the adopted processing algorithm, but the minimum measurement time can be independently estimated, as detailed in the following. Regarding the first approach, that is the impedance analyzer of [8], the relevant parameters of the impedance analyzer are the delay time (Dl) and the integration time (IT). As sketched in Fig. 3, the Dl is the time needed to stabilize the response after the frequency change (it can be set from 0 to 10^5 s); the IT defines the time interval during which the analyzer measures the input signals. It is fundamental for the rejection of harmonics and noise (it can set from 10 ms to 10^5 s). To compute the minimum time required to measure the thickness, we considered a minimum value of 10 ms for the IT, a value of Dl corresponding to four periods of the excitation waveform, which represents the minimum number of periods to get a stable response after the frequency changes and excluding the time to acquire and process the signals. Table III shows the minimum thickness measurement time MMT_{IMP} using the impedance analyzer for three different values (2, 5, and 10 Hz) of frequency resolution. Specifically, a frequency resolution of $\Delta f = 5$ Hz requires 12.96 s.

Regarding the second approach, a delay time equal to the previous one and a variable integration time equal to two periods of the considered excitation frequency, corresponding to the minimum number of periods to extract the desired quantities from the signals, have been considered. Using these

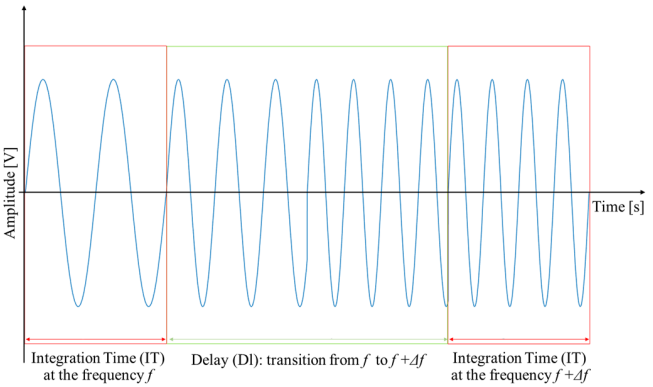

Fig. 3. Representation of integration time (IT) and delay (Dl) in a swept-sine application during the transition from the frequency f to the frequency $f + \Delta f$ (where Δf is the chosen frequency resolution).

TABLE III

ANALYSIS OF MINIMUM THICKNESS MEASUREMENT TIME USING BOTH AN IMPEDANCE ANALYZER (MMT_{IMP}) OR A GENERAL-PURPOSE DEVICE (MMT_{GP}) IN A FREQUENCY RANGE FROM 100 Hz TO 5 kHz

Δf [Hz]	MMT_{IMP} [s] (1)	MMT_{GP} [s] (2)
2	32.35	11.76
5	12.96	9.10
10	6.49	7.17

(1) evaluated for a Delay (Dl) = 4 periods of the excitation waveform and an Integration Time (IT) = 10 ms as for the specification of the impedance meter
(2) evaluated for a Delay (Dl) = 4 periods and an Integration Time (IT) = 2 periods of the excitation waveform.

values for Dl and IT, the minimum thickness measurement time MMT_{GP} using the general-purpose device is evaluated and shown in Table III, for the three considered values of frequency resolution. Table III shows a minimum thickness measurement time of about 9.1 s required at $\Delta f = 5$ Hz. In any case, even decreasing the frequency resolution to $\Delta f = 10$ Hz, the minimum measurement time under these ideal conditions is never less than 6.49 s. Despite these measurement times have been obtained under ideal conditions (e.g., considering minimum number of signal cycle to be processed, zero processing time, etc.), they cannot be considered proper in online controls in production processes.

A solution to reduce the measurement time is the use of multifrequency signals processed by fast Fourier transform (FFT), as mentioned also by the authors of [9]. The general expression of a multisine signal is

$$I(t) = \sum_{k=1}^{N_S} \sqrt{2} \cdot I_k \cdot \sin\left(2 \cdot \pi \cdot f_k \cdot t + \varphi_k\right) \tag{13}$$

where I_k, f_k, and φ_k are the root mean square (rms), frequency, and phase of the k-th sinusoid, and N_s is the total number of tones.

Under the same conditions of the previous analysis of the measurement time (frequency range from 100 to 5000 Hz and frequency resolution of 5 Hz), the multifrequency excitation current signal is composed by a high number of tones ($N_S = 981$). The total rms value (I_{RMS}) of the excitation current is given by

$$I_{\mathrm{RMS}} = \sqrt{\sum_{k=1}^{N_S} I_k^2}. \tag{14}$$

If the multisine signal is composed by tones with equal rms values, then the total rms value of the excitation current is equal to $I_{\mathrm{RMS}} = \sqrt{N_S} \cdot I_k$. This means that for a prescribed total rms current value I_{RMS}, the rms current value for each tone is equal to $I_k = I_{\mathrm{RMS}}/\sqrt{N_S}$; for instance, for $I_{\mathrm{RMS}} = 100$ mA, we have $I_k \cong 3$ mA. Therefore, a multisine signal aimed to reduce the measurement time needs to be accurately designed to get a suitable tradeoff among number of tones, i.e., frequency resolution, maximum rms value of the total excitation current, and minimum rms value of each tone. It is worth noting that the maximum rms is limited by the maximum current supported by both the excitation coil and the driving electronics, that is particularly relevant for portable instrumentation supplied by batteries. Similarly, the minimum rms per each tone is relevant in order to get a proper stimulus of the material at that specific tone.

In Section III, it will be shown the proposal for the reduction of the measurement time in thickness estimation by using both a suitable double step multifrequency approach and a proper interpolation method.

III. Proposed Measurement Method

As shown in Section II, in view of industrial applications, the method proposed in [8] has two main challenges to be faced: the measurement time and the accuracy. In this section, we address these challenges.

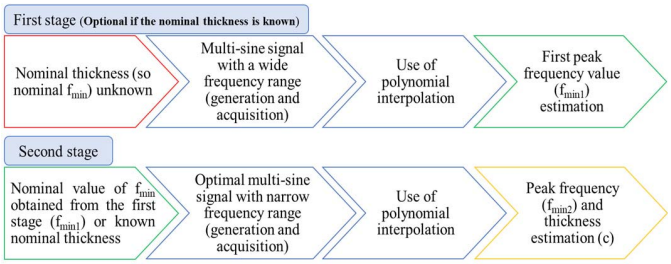

Fig. 4. Operation flowchart behind the dual-stage strategy.

To speed up the measurement method and to improve the accuracy in evaluating the thickness of metallic plates, multisine signals can be adopted. However, the maximum number of tones to be used is limited by the total rms value of the excitation signal because of sensor heating and power consumption, which represent a major drawback in battery powered instrumentation. For these reasons, the choice of a proper number of tones, combined with frequency interpolation techniques, is mandatory.

Specifically, to take into account the finite frequency resolution of the multisine signals and to improve the accuracy of the measurement method, various interpolating polynomials have been analyzed and applied in this work. The ultimate goal is to get a more accurate estimation of the value of the peak frequency. The interpolation techniques we propose have been firstly developed and validated by means of numerical simulations and, then, tested experimentally.

For a further improvement of the thickness measurement accuracy, the use of a double stage of excitation and processing is proposed in this article, as shown in the flowchart of Fig. 4. In particular, the dual-stage procedure is organized as follows: 1) in a first stage, the goal is to find the range where the peak frequency (f_{min1}) is located, by using a multisine signal with a wide frequency range (this first step is optional and can be jumped if the nominal thickness and, consequently, the f_{min1} value is *a priori* known); and 2) in a second stage, we proceed with a multisine signal over a narrow and optimized frequency range centered on the estimate of the peak frequency (f_{min1}), obtained in the first step or known *a priori* from the knowledge of the nominal thickness of the sample. In the first stage the frequencies are allocated on a logarithmic scale, whereas in the second stage, they are distributed uniformly. In both stages, interpolating polynomials are essential to filter the noisy measurements and interpolate the data to get an accurate estimate of the peak position. Adopting this dual-stage strategy, the resulting measurement time is less than 3 s.

In the following subsections, the proposed multifrequency signals and the related interpolation methods are analyzed and discussed in detail.

A. Multifrequency Signal Generation

According to [12], [13], if the phase φ_k appearing in (13) is given by

$$\varphi_k = -\pi \cdot \frac{k(k-1)}{N_s}, \tag{15}$$

then the resulting signal exhibits a quite constant envelope, which is an essential feature for optimizing both the peak amplitude of the current delivered to the exciting probe and the full scale of the analog to digital converter of the acquisition board [12], [13].

The choice of the number of tones for each stage aims to balance the energy content of the excitation signal (limited by the peak power of the probe and/or by the whole measurement system) and the number of frequency points required to get a proper accuracy in estimating the peak frequency.

In the first stage, a signal with a lower energy content has been considered, since we only need to estimate the frequency range where the peak occurs. On the contrary, in the second stage, the frequency range of interest is smaller, and so is the number of required tones. Therefore, we can increase the rms value for each single tone of the excitation signal.

For the chosen setup, which will be described in detail in the following section, two different excitation signals have been designed. For the first stage, a 19-tones multisine signal has been designed with a semi-logarithmic frequency distribution over the range 100–5000 Hz. As aforementioned, this frequency range is suitable for samples with thicknesses ranging from 0.35 to 6 mm (at σ equal to 18 MS/m) or samples with thicknesses ranging from 0.1 to 5 mm (at σ equal to 59 MS/m).

For the second stage, an 11-tone multisine signal has been designed. The center frequency of the multisine signal is that of the peak found either in the first stage, or that arising from the nominal value of the thickness. The multisine signal covers a frequency range from -30% to $+30\%$ of the center frequency.

B. Interpolation Techniques

The reduction in the number of selected frequency points can be leveraged by using proper interpolating polynomials. The choice of the optimal interpolating polynomial allows to obtain higher performances in the estimation of the value of the peak frequency and, therefore, of the thickness of the specimen.

In this work, four different types of interpolation techniques have been considered:

1) Fourth-order interpolating polynomial (FOIP);
2) Fourth-order Chebyshev interpolating polynomial (FOCIP);
3) Modified Akima interpolator polynomial (MAIP);
4) Piecewise cubic Hermite interpolator polynomial (PCHIP).

It is worth to highlight that, for comparison purposes, two different classes of interpolation techniques have been considered. The first class (including FOIP and FOCIP) uses the entire dataset to determine the polynomial equation, while the second class (including MAIP and PCHIP) determines the polynomial equation not considering the entire dataset, but divides it into many subsets where the polynomial equation is determined (piecewise interpolation techniques). In the following, some features about the analyzed interpolation techniques are provided (more detailed information can be found in the given references).

A basic interpolating polynomial consists in the interpolation of a given dataset by the polynomial of the lowest possible degree passing through all the points of the dataset. An FOIP has been chosen for this study, given the number of points available for the dataset and the resulting R-squared values (closest to the unit) and the lowest root-mean-square error values.

Accordingly, the resulting fourth-order polynomial can be defined as in the following equation:

$$p_4(\mathrm{x}) = a_4x^4 + a_3x^3 + a_2x^2 + a_1x + a_0 \tag{16}$$

where $a_0, \ldots, a_4$ are the coefficients of the equation, x is the unknown variable, and $p_4(x)$ is the interpolation polynomial.

The Chebyshev interpolating polynomial is a sequence of orthogonal polynomials related to De Moivre's formula [21], with several properties that make them extremely useful when approximating functions are investigated. An FOCIP has been chosen for this study, to compare the same order polynomial interpolations. As a result, the FOCIP formulation given in the following has been used:

$$p_4(x) = U_4^*(x) = \frac{\sin(5\theta)}{\sin(\theta)}$$
$$\text{with} \quad \cos(\theta) = \frac{2x - (a+b)}{b-a} \quad \text{and} \quad \theta\epsilon[0, \pi] \tag{17}$$

being $U_4^*(x)$ the second-kind Chebyshev polynomial of 4th degree, and $x\epsilon I$ the unknown variable defined over the interval $I = [a, b]$.

The Akima interpolating algorithm performs cubic interpolations to realize piecewise polynomials with continuous first-order derivatives [22], [23]. The MAIP algorithm avoids excessive local ripples and, unlike the classic Akima algorithm, assigns an average weight to the points on both sides, to avoid possible undulation phenomena. The interpolating expression for a portion of curve between two consecutive points can be found in [22]. If we have an interval between two points (x_1, y_1) and (x_2, y_2), being t_1, t_2 the slopes at these two points, a third-degree polynomial can be uniquely determined, as in the following equation:

$$p(x) = a_0 + a_1(x - x_1) + a_2(x - x_1)^2 + a_3(x - x_1)^3 \tag{18}$$

where

$$a_0 = y_1, \tag{19}$$
$$a_1 = t_1, \tag{20}$$
$$a_2 = \frac{[3(y_2 - y_1)/(x_2 - x_1) - 2t_1 - t_2]}{(x_2 - x_1)}, \tag{21}$$
$$a_3 = \frac{[t_1 + t_2 - 2(y_2 - y_1)/(x_2 - x_1)]}{(x_2 - x_1)^2}. \tag{22}$$

The cubic Hermite interpolator PCHIP is a spline where each piece is a specified third-degree polynomial in the form of Hermite, i.e., by its values and first derivatives at the end points of the corresponding domain interval [24]. Let $\pi : a = x_1 < x_2 < \cdots < x_n = b$ be a partition of the interval $I = [a, b]$. Let $\{f_i : i = 1, 2, \ldots, n\}$ be a given set of monotone data values at the partition points. For instance, let us assume $f_i \leq f_{i+1} (i = 1, 2, \ldots, n-1)$. It can be constructed on π a

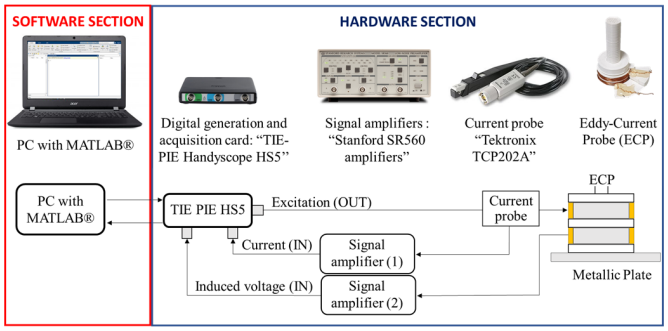

Fig. 5. Schematic block diagram of the adopted measurement setup.

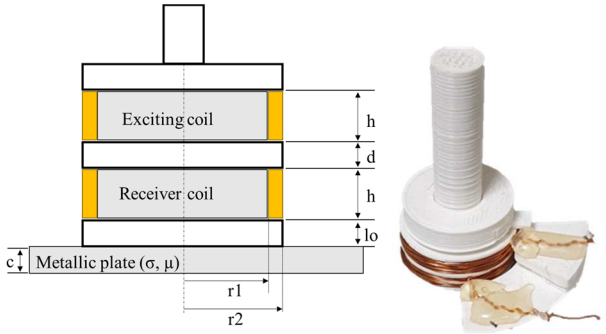

(a) (b)

Fig. 6. Coils geometry. (a) Schematic of the two coaxial coils placed on the metallic plate. (b) Photo of the realized probe adopted for the experimental measurements.

piecewise cubic function $p(x)$, such that, in each subinterval $I_i = [x_i, x_{i+1}]$, $p(x)$ is a cubic polynomial represented as in the following equation:

$$p(x) = f_i H_1(x) + f_{i+1} H_2(x) + d_i H_3(x) + d_{i+1} H_4(x) \quad (23)$$

where

$$d_j = p'(x_j) \text{ for } j = i, i+1 \quad (24)$$

and $H_k(x)$, for $k = 1, \ldots, 4$, are the so-called cubic Hermite basis function for the interval I_i [24].

All these interpolation techniques are already existing in MATLAB®, and can be easily coded by means of the following functions:

1) FOIP [25]:

$$p = fit(f_{\text{vet}}, \Delta R/\omega, \text{'poly4'});$$

2) FOCIP [26]:

$$p = chebFitLs(f_{\text{vet}}, \Delta R/\omega, [min(f_{\text{vet}}), \max(f_{\text{vet}})], 4);$$

3) MAIP [27]:

$$p = interp1(f_{\text{vet}}, \Delta R/\omega, f_{\text{vet\_hr}}, \text{'makima'});$$

4) PCHIP [27]:

$$p = interp1(f_{\text{vet}}, \Delta R/\omega, f_{\text{vet\_hr}}, \text{'pchip'}),$$

where f_{vet} is the vector of frequency components of the considered multifrequency signal, and $f_{\text{vet\_hr}}$ is a vector of frequencies linearly ranging from $\min(f_{\text{vet}})$ and $\max(f_{\text{vet}})$ with a resolution step of 1 Hz.

IV. Experimental Setup and Considered Case Studies

A. Experimental Setup Description

A schematic block diagram of the measurement setup is shown in Fig. 5. The measurement station comprises a hardware section and a software section. The hardware section is composed by the following components: a digital generation and acquisition card, two signal amplifiers, a current probe, and the eddy-current probe (ECP). The ECP consists of two coaxial coils, one used as exciting coil and one as receiver coil. The coils geometry is shown in detail in Fig. 6 and their dimensions are listed in Table IV.

TABLE IV
Coils Parameters

r_1 [mm]	11.8
r_2 [mm]	12.4
l_o (lift-off) [mm]	0.5
h (height) [mm]	3
d (gap) [mm]	1
Number of turns (N_1=N_2)	20

A TIE-PIE Engineering Handyscope HS5-540XMS-W5™ digital scope card is used to provide the excitation current to the exciting coil and to acquire the desired signals at 14 bits and a sampling frequency of 100 kHz. The excitation current has been sensed by means of a current probe Tektronix TCP202A and both the sensed excitation current and the output voltage on receiver coil were conditioned using two SR560 Stanford Research System low-noise amplifiers before sending them to the TIE-PIE acquisition channels.

The tests have been carried out by feeding the exciting coil with a multisine signal that, as described in Section III-A, is composed by 19 tones (with total rms value of the excitation current equal to 18 mA) or 11 tones (with a total rms value ranging from 15 to 80 mA depending on the frequency range to be used in this stage).

The software section includes a MATLAB® algorithm running on a dual-core system PC [Intel(R) Core (TM) CPU at 2.70 GHz and 12-GB RAM), which manages the TIE-PIE in the generation/acquisition of the multisine signals and allows the processing of the acquired data.

B. Considered Case Studies

The experimental tests have been carried out considering six reference aluminum plates, whose actual thickness values and main characteristics are listed in Table V. Five EN AW-1050A aluminum plates with different thicknesses from 0.5 to 4 mm, and one 2024T3 aluminum plate with thickness of 2.003 mm have been used. The electrical conductivities of the various plates were measured by the Hocking Phasec 2d® [28].

TABLE V
MAIN CHARACTERISTICS OF THE CONSIDERED ALUMINUM PLATES

Metal alloy	Plate #	Actual thickness [mm]	Electrical conductivity [MS/m]	Plate Dimensions [cm x cm]
EN AW-1050A (Metallog)	1	0.469	35.4	13 x 18
	2	1.035	35.3	25 x 25
	3	1.969	35.0	25 x 50
	4	2.912	35.3	25 x 25
	5	3.994	34.5	25 x 25
2024T3 (Casoni)	6	2.003	18.8	20 x 20

V. NUMERICAL (SIMULATION) RESULTS

In this section, we carry out an analysis of the performances of the proposed thickness measurement method. Specifically, this evaluation has been carried out by combining model (1)–(11) of Section II-A with the statistical description of the experimental noise which is described in Section V-A. The aim is to produce realistic "synthetic" data to predict the trend of the performances given by different interpolating polynomials and the two-stage multifrequency approach.

To compare the performances, we use the classical percentage error (RTE) defined as

$$\mathrm{RTE} = 100 \cdot \frac{c_e - c_a}{c_a} \tag{25}$$

where c_a is the actual thickness of the sample and c_e is the estimate following from (12).

Then, the two-stage simulation was repeated using a multifrequency signal and different interpolating polynomials have been applied to improve the estimate of the peak frequency. Finally, the estimated thickness c_e and the relative thickness error RTE were estimated at the second stage. The remaining part of this section is organized as follows: first (Section V-A), we evaluate the average value and the standard deviation of the noise, as a function of the frequency. Then (Section V-B), simulations without the noise are carried out to check the performances of the interpolation methods in ideal (noise-free) conditions. Finally (Section V-C), numerical data have been contaminated with synthetic noise to assess the potential impact of the measurement noise on the results.

A. Noise Characterization of the Experimental Setup

In this section, the noise characterization for the measurement setup is discussed. The aim is to estimate the typical experimental noise to implement very realistic numerical simulations to predict the performances of different interpolation algorithms, as described in Section III-B.

The characterization is made using the measurement station described in Section IV-A. A series of 100 repeated tests in a realistic experimental setting has been performed. The probe is placed both in air and on a planar metallic plate, for all plates of Table V. The acquired current and voltage signals have been processed to estimate the mutual impedance when the probe is over the plate ($\dot{Z}_{m,\mathrm{plate}}(f)$) and in air ($\dot{Z}_{m,\mathrm{air}}(f)$), and, then, $\Delta R/\omega$ [see (11)].

Fig. 7 shows an example of the distribution of $\Delta R/\omega$ for a specific frequency (125 Hz) and for a specific plate (thickness of 2.003 mm).

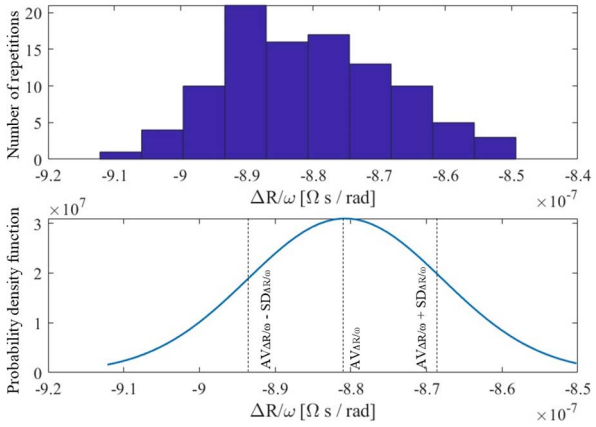

Fig. 7. Experimental distribution of $\Delta R/\omega$ at a prescribed frequency.

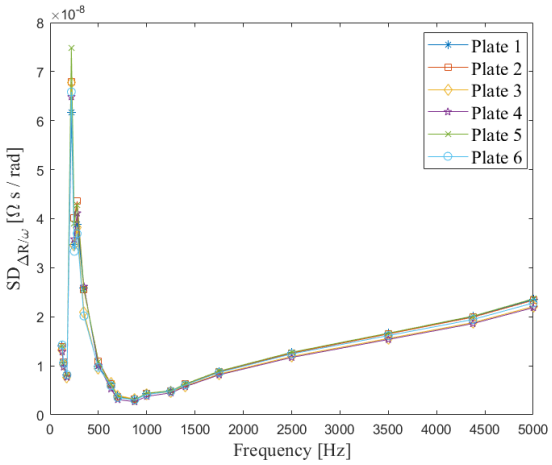

Fig. 8. Standard deviation (SD) of $\Delta R/\omega$ versus frequency.

As it is possible to note, the noise due to the overall measurement setup on the single tone can be described by a Gaussian distribution of proper average value ($\mathrm{AV}_{\Delta R/\omega}$) and standard deviation ($\mathrm{SD}_{\Delta R/\omega}$).

Fig. 8 shows the behavior of $\mathrm{SD}_{\Delta R/\omega}$ for all the considered frequencies and for all the plates under analysis. As expected, the $\mathrm{SD}_{\Delta R/\omega}$ depends on the frequency. Specifically, it shows higher values at higher frequency. Indeed, since we are driving the coil with a voltage-controlled signal, higher frequencies correspond to lower (coil) currents. This trend changes at lower frequencies (near 250 Hz) because of the environmental noise.

B. Simulation Results Without Measurement Noise

As concerns the first stage of the procedure aforementioned, the estimated thickness and the resulting RTE have been calculated and listed in Table VI. It can be noticed that, generally, piecewise interpolating polynomials (MAIP, PCHIP) allow obtaining better performances than the simpler interpolating polynomials (FOIP, FOCIP). The best performance with RTE, always lower than 3%, can be observed for the MAIP interpolation technique. The peak frequency estimated

TABLE VI
PERFORMANCES OBTAINED IN SIMULATION BY USING THE 19-TONE MULTISINE SIGNAL (FIRST STAGE)

FOIP			FOCIP		MAIP		PCHIP	
Actual thickness [mm]	Estimated thickness [mm]	RTE [%]	Estimated thickness [mm]	RTE [%]	Estimated thickness [mm]	RTE [%]	Estimated thickness [mm]	RTE [%]
0.469	0.491	4.76	0.489	4.31	0.478	1.93	0.526	12.24
1.035	0.859	-16.97	0.783	-24.36	1.033	-0.22	1.076	4.00
1.969	1.325	-32.70	1.058	-46.28	1.989	1.01	1.961	-0.40
2.003	1.661	-17.08	1.509	-24.66	1.993	-0.48	2.094	4.53
2.912	2.743	-5.82	1.728	-40.67	2.988	2.59	2.962	1.71
3.994	8.819	120.80	8.819	120.80	3.994	0	3.937	-1.43

TABLE VII
PERFORMANCES OBTAINED IN SIMULATION BY USING THE 11-TONE MULTISINE SIGNAL (SECOND STAGE)

FOIP			FOCIP		MAIP		PCHIP	
Actual thickness [mm]	Estimated thickness [mm]	RTE [%]	Estimated thickness [mm]	RTE [%]	Estimated thickness [mm]	RTE [%]	Estimated thickness [mm]	RTE [%]
0.469	0.470	0.16	0.470	0.21	0.470	0.32	0.470	0.16
1.035	1.035	0	1.035	0	1.030	-0.44	1.013	-2.15
1.969	1.965	-0.20	1.965	-0.20	1.969	0	1.965	-0.20
2.003	2.000	-0.15	2.000	-0.15	1.991	-0.58	1.970	-1.65
2.912	2.945	1.14	2.953	1.43	2.953	1.43	2.953	1.43
3.994	3.994	0	3.994	0	3.980	-0.36	3.909	-2.13

using MAIP is used as center frequency to define the frequency range for the second stage.

As concerns the second-stage procedure described above, the final estimated thickness and the resulting RTE have been reported in Table VII. In this case, FOIP and FOCIP techniques show better performances than piecewise interpolation techniques (MAIP, PCHIP). This is due to their working principles giving better performances when the minimum of the interpolated function is about in the center of the range of interest. Indeed, in the second stage, the frequency span in the considered case is centered with respect to the peak frequency from the first stage.

C. Simulation Results With Measurement Noise

The effect of the considered interpolation techniques on the performance of the proposed thickness measurement method was analyzed also in presence of the typical noise introduced by the measurement setup.

To consider the typical noise, the simulated values of $\Delta R/\omega$ for each frequency were corrupted using a normal distribution with mean parameter $AV_{\Delta R/\omega}$ and standard deviation $SD_{\Delta R/\omega}$ (as from Section V-A). This procedure was repeated 100 times and both the mean value (RTE_M) and the standard deviation (SD_{RTE}) of the obtained RTE values were evaluated.

As expected, there was a general performance degradation due to the presence of noise (see Tables VIII and IX).

The relative performances between MAIP, PCHIP, FOIP, and FOCIP interpolating polynomials were the same as for the study without noise. Specifically, it is possible to observe that the performance of FOIP and FOCIP is less sensitive to the noise (smaller SD_{RTE}), but the RTE is worse than that from MAIP and PCHIP, as shown in Table VIII. On the contrary, at the second stage, the values of the RTE from FOIP and FOCIP are comparable with those from MAIP and PCHIP but FOIP and FOCIP gave better repeatability, i.e., smaller SD_{RTE}. Summing up, the optimal choice is an MAIP or a PCHIP for the first stage, and an FOIP or an FOCIP for the second stage.

VI. EXPERIMENTAL RESULTS

In this section, the experimental results achieved by using the proposed method are presented and discussed. The experimental campaign was made using the measurement station and the specimens described in Sections IV-A and IV-B.

The tests carried out at simulation level were repeated experimentally for final validation, in the same conditions.

From the results in Section V-C, MAIP and PCHIP were applied at the first stage, while FOIP and FOCIP were applied at the second stage. Each test was repeated 100 times and both the mean value (RTE_M) and the standard deviation (SD_{RTE}) were evaluated. Experimental results for the first and second stages are shown in Tables X and XI, respectively. They confirm performances predicted on synthetic data with noise (see Tables VIII and IX).

From Table X, it follows that MAIP and PCHIP have similar performances in terms of both the RTE_M and the SD_{RTE}. Then, the peak frequency estimated by using MAIP was used as center frequency for the second stage. Similar results can be achieved by means of PCHIP.

From Table XI, it follows that FOIP and FOCIP have similar performances at the second stage. More precisely, FOCIP interpolating polynomials appears to show slightly better performances with maximum RTE lower than 2.7%, and a maximum standard deviation of 0.7%.

Eventually, an analysis of the measurement time is showed in Table XII. The time required to each elementary phase

TABLE VIII

PERFORMANCES OBTAINED IN SIMULATION INTRODUCING THE TYPICAL NOISE OF SETUP AND USING 19 FREQUENCIES (FIRST STAGE)

FOIP				FOCIP			MAIP			PCHIP		
Actual thickness [mm]	Estimated thickness [mm]	RTE_M [%]	SD_{RTE} [%]	Estimated thickness [mm]	RTE_M [%]	SD_{RTE} [%]	Estimated thickness [mm]	RTE_M [%]	SD_{RTE} [%]	Estimated thickness [mm]	RTE_M [%]	SD_{RTE} [%]
0.469	0.490	4.59	0.11	0.490	4.09	0.10	0.529	12.79	0.59	0.526	10.99	0.58
1.035	0.855	-16.94	0.08	0.782	-24.35	0.09	1.079	0.20	0.37	1.076	0.89	0.56
1.969	1.340	-32.82	0.09	1.061	-46.41	0.56	1.864	-0.65	0.71	1.961	-0.58	0.10
2.003	1.672	-16.94	0.07	1.513	-24.54	0.08	2.111	0.38	0.39	2.094	1.02	0.59
2.912	2.658	-8.72	0.77	1.769	-40.87	0.31	2.979	2.30	2.19	2.962	1.72	2.15
3.994	8.819	120.80	0	8.819	120.80	0	3.662	-6.08	1.34	3.937	-1.42	1.32

TABLE IX

PERFORMANCES OBTAINED IN SIMULATION INTRODUCING THE TYPICAL NOISE OF SETUP AND USING 11 FREQUENCIES (SECOND STAGE)

FOIP				FOCIP			MAIP			PCHIP		
Actual thickness [mm]	Estimated thickness [mm]	RTE_M [%]	SD_{RTE} [%]	Estimated thickness [mm]	RTE_M [%]	SD_{RTE} [%]	Estimated thickness [mm]	RTE_M [%]	SD_{RTE} [%]	Estimated thickness [mm]	RTE_M [%]	SD_{RTE} [%]
0.469	0.478	-0.68	0.36	0.468	-0.97	0.45	0.496	-0.35	0.56	0.496	-0.40	0.58
1.035	1.051	0.10	0.16	1.061	0.15	0.20	1.075	-0.71	0.39	1.074	-0.52	0.40
1.969	1.961	0.02	0.08	1.942	0.06	0.13	2.018	1.31	0.26	2.091	1.33	0.27
2.003	2.024	0.11	0.21	2.038	0.31	0.26	1.970	-0.44	0.40	1.970	-0.42	0.43
2.912	2.928	1.30	0.05	2.937	1.28	0.08	2.787	0.60	0.34	2.787	0.46	0.34
3.994	3.951	-0.21	0.15	3.951	-0.19	0.23	4.129	0.46	0.30	4.160	0.66	0.35

TABLE X

EXPERIMENTAL PERFORMANCES OBTAINED USING THE 19-TONE MULTISINE SIGNAL (FIRST STAGE)

FOIP				FOCIP			MAIP			PCHIP		
Actual thickness [mm]	Estimated thickness [mm]	RTE_M [%]	SD_{RTE} [%]	Estimated thickness [mm]	RTE_M [%]	SD_{RTE} [%]	Estimated thickness [mm]	RTE_M [%]	SD_{RTE} [%]	Estimated thickness [mm]	RTE_M [%]	SD_{RTE} [%]
0.469	0.487	3.84	0.04	0.486	3.67	0.03	0.527	12.43	0.05	0.526	12.17	0
1.035	0.871	-15.84	0.09	0.805	-22.18	0.05	1.097	5.95	0.04	1.077	4.01	0
1.969	1.395	-29.14	0.28	1.106	-43.82	0.13	2.043	3.76	0.52	1.991	1.12	0.57
2.003	1.666	-16.71	0.15	1.544	-22.79	0.10	2.118	5.74	0.05	2.094	4.53	0
2.912	3.479	19.49	3.75	1.813	-37.74	1.07	2.995	2.84	1.27	2.892	-0.68	1.26
3.994	8.819	120.82	0	8.819	120.82	0	3.923	-1.77	1.45	3.921	-1.83	1.47

TABLE XI

EXPERIMENTAL PERFORMANCES OBTAINED USING THE 11-TONE MULTISINE SIGNAL (SECOND STAGE)

FOIP				FOCIP			MAIP			PCHIP		
Actual thickness [mm]	Estimated thickness [mm]	RTE_M [%]	SD_{RTE} [%]	Estimated thickness [mm]	RTE_M [%]	SD_{RTE} [%]	Estimated thickness [mm]	RTE_M [%]	SD_{RTE} [%]	Estimated thickness [mm]	RTE_M [%]	SD_{RTE} [%]
0.469	0.479	2.22	0.13	0.461	-1.62	0.13	0.461	-1.62	0.56	0.460	-1.92	0.12
1.035	1.068	3.19	0.12	1.063	2.70	0.12	1.069	3.28	0.38	1.073	3.68	0
1.969	1.993	1.23	0.22	1.977	0.42	0.21	2.008	1.97	0.36	2.007	1.94	0.61
2.003	2.045	2.08	0.12	2.036	1.63	0.11	2.054	2.69	0.12	2.087	4.33	0
2.912	2.868	-1.52	0.06	2.901	-0.39	0.09	2.884	-0.96	0.14	2.884	-0.96	0
3.994	4.009	0.37	0.57	3.923	-1.77	0.74	4.098	2.61	0.74	4.160	4.16	1.14

is evaluated: generation, acquisition, and processing time for both the first and the second stages. It worth noting that the measurement of $\dot{Z}_{m,\mathrm{air}}(f)$ can be carried out once for all, before the signal generation and/or acquisition. For this reason, the related time has not been accounted in Tables III and XII. From the measurement time showed in Table XII, it follows that the proposed method requires up to 2.66 s, when using the double stage approach.

Moreover, the accuracy obtained by applying the proposed method, after the second measurement stage, is in line with both the requirements of the DS EN 485-4:2000 standard [1] and the results shown in [8]. These results have been achieved for treating automatically a "large" range of thicknesses of interest (from 0.4 to 4 mm, about), where the double stage procedure is mandatory to get a proper accuracy. Under these conditions (large thicknesses range, two stage procedure), the

TABLE XII
TIME PERFORMANCE OF THE PROPOSED MEASUREMENT TECHNIQUE

Generation and acquisition – first stage	1.41 s
Elaboration – first stage	0.06 s
Generation and acquisition – second stage	1.14 s
Elaboration – second stage	0.05 s
Total Time	2.66 s

proposed method requires less than 2.7 s, suitable for the on-line test during typical production processes. When the nominal thickness value is given, then only the second stage can be applied. This requires a measurement time lower than 1.2 s.

Summing up, the experimental results confirm the accuracy and efficiency of the proposed method.

VII. CONCLUSION

In this work, we presented an accurate and efficient measurement method based on [8], proper for almost real-time applications, such as those involved in industrial applications.

Specifically, the proposed approach allows to improve the performances of [8] in terms of both measurement time and range of applicability: thanks to the dual-stage strategy, one can treat thickness in a wider range. In particular, the first stage provides a coarse estimate of the thickness, whereas the second one provides its accurate estimate. Interpolating polynomial and multifrequency signals played a relevant role in reducing the overall measurement time.

REFERENCES

[1] *EN 485-4:2000*. Accessed: Jul. 13, 2022. [Online]. Available: https://infostore.saiglobal.com/en-gb/standards/ds-en-485-4-2000-462686_saig_ds_ds_1042214/

[2] J. Ren, Z. Jian, X. Wang, R. Mingjun, L. Zhu, and X. Jiang, "Complex surface reconstruction based on fusion of surface normals and sparse depth measurement," *IEEE Trans. Instrum. Meas.*, vol. 70, pp. 1–13, 2021, doi: 10.1109/TIM.2021.3061264.

[3] Y.-M. Choi, H. Yoo, and D. Kang, "Large-area thickness measurement of transparent multi-layer films based on laser confocal reflection sensor," *Measurement*, vol. 153, Mar. 2020, Art. no. 107390.

[4] R. Raisutis, R. Kazys, and L. Mazeika, "Ultrasonic thickness measurement of multilayered aluminum foam precursor material," *IEEE Trans. Instrum. Meas.*, vol. 57, no. 12, pp. 2846–2855, Dec. 2008, doi: 10.1109/TIM.2008.927208.

[5] M. Bramanti, "A nondestructive diagnostic method based on swept-frequency ultrasound transmission-reflection measurements," *IEEE Trans. Instrum. Meas.*, vol. 41, no. 4, pp. 490–494, Aug. 1992, doi: 10.1109/19.155913.

[6] G. Betta *et al.*, "Thickness measurements with eddy current and ultrasonic techniques," in *Sensors Microsystems* (Lecture Notes in Electrical Engineering), vol. 629, G. D. Francia, Eds. Cham, Switzerland: Springer, 2019, pp. 387–394.

[7] A. V. Egorov *et al.*, "Inspection of aluminum alloys by a multi-frequency eddy current method," *Defense Technol.*, vol. 11, no. 2, pp. 99–103, Jun. 2015.

[8] W. Yin and A. J. Peyton, "Thickness measurement of non-magnetic plates using multi-frequency eddy current sensors," *NDT E Int.*, vol. 40, no. 1, pp. 43–48, Jan. 2007.

[9] M. Lu, L. Yin, A. J. Peyton, and W. Yin, "A novel compensation algorithm for thickness measurement immune to lift-off variations using eddy current method," *IEEE Trans. Instrum. Meas.*, vol. 65, no. 12, pp. 2773–2779, Aug. 2016.

[10] W. Yin and K. Xu, "A novel triple-coil electromagnetic sensor for thickness measurement immune to lift-off variations," *IEEE Trans. Instrum. Meas.*, vol. 65, no. 1, pp. 164–169, Jan. 2016, doi: 10.1109/TIM.2015.2479106.

[11] C. V. Dodd and W. E. Deeds, "Analytical solutions to eddy-current probe-coil problems," *J. Appl. Phys.*, vol. 39, no. 6, pp. 2829–2838, May 1968.

[12] A. Bernieri, G. Betta, L. Ferrigno, and M. Laracca, "Multi-frequency eddy current testing using a GMR based instrument," *Int. J. Appl. Electromagn. Mech.*, vol. 39, nos. 1–4, pp. 355–362, Sep. 2012.

[13] A. Bernieri, G. Betta, L. Ferrigno, M. Laracca, and S. Mastrostefano, "Multifrequency excitation and support vector machine regressor for ECT defect characterization," *IEEE Trans. Instrum. Meas.*, vol. 63, no. 5, pp. 1272–1280, May 2014, doi: 10.1109/TIM.2013.2292326.

[14] J. García-Martín, J. Gómez-Gil, and E. Vázquez-Sánchez, "Non-destructive techniques based on eddy current testing," *Sensors*, vol. 11, no. 3, pp. 2525–2565, Feb. 2011.

[15] E. Pinotti and E. Puppin, "Simple lock-in technique for thickness measurement of metallic plates," *IEEE Trans. Instrum. Meas.*, vol. 63, no. 2, pp. 479–484, Feb. 2014, doi: 10.1109/TIM.2013.2278999.

[16] W. Cheng, "Thickness measurement of metal plates using swept-frequency eddy current testing and impedance normalization," *IEEE Sensors J.*, vol. 17, no. 14, pp. 4558–4569, Jul. 2017, doi: 10.1109/JSEN.2017.2710356.

[17] H. Wang, J. Huang, L. Liu, S. Qin, and Z. Fu, "A novel pulsed eddy current criterion for non-ferromagnetic metal thickness quantifications under large liftoff," *Sensors*, vol. 22, no. 2, p. 614, Jan. 2022, doi: 10.3390/s22020614.

[18] M. Fan, B. Cao, A. I. Sunny, W. Li, G. Tian, and B. Ye, "Pulsed eddy current thickness measurement using phase features immune to liftoff effect," *NDT E Int.*, vol. 86, no. 3, pp. 123–131, 2017, doi: 10.1016/j.ndteint.2016.12.003.

[19] M. Fan, B. Cao, G. Tian, B. Ye, and W. Li, "Thickness measurement using liftoff point of intersection in pulsed eddy current responses for elimination of liftoff effect," *Sens. Actuators A, Phys.*, vol. 251, pp. 66–74, Nov. 2016, doi: 10.1016/j.sna.2016.10.003.

[20] G. Y. Tian and A. Sophian, "Reduction of lift-off effects for pulsed eddy current NDT," *NDT E Int.*, vol. 38, no. 4, pp. 319–324, 2005, doi: 10.1016/j.ndteint.2004.09.007.

[21] M. R. Eslahchi, M. Dehghan, and S. Amani, "The third and fourth kinds of Chebyshev polynomials and best uniform approximation," *Math. Comput. Model.*, vol. 55, nos. 5–6, pp. 1746–1762, Mar. 2012.

[22] H. Akima, "A new method of interpolation and smooth curve fitting based on local procedures," *J. ACM*, vol. 17, no. 4, pp. 589–602, Oct. 1970.

[23] H. Akima, "A method of bivariate interpolation and smooth surface fitting based on local procedures," *Commun. ACM*, vol. 17, no. 1, pp. 18–20, Jan. 1974.

[24] F. N. Fritsch and R. E. Carlson, "Monotone piecewise cubic interpolation," *SIAM J. Numer. Anal.*, vol. 17, no. 2, pp. 238–246, 1980.

[25] MathWorks. *'Fit' Function*. Accessed: Jul. 13, 2022. [Online]. Available: https://it.mathworks.com/help/curvefit/fit.html

[26] M. P. Kelly. *Chebyshev Polynomials*. Accessed: Jul. 13, 2022. [Online]. Available: https://github.com/MatthewPeterKelly/Chebyshev_Polynomials

[27] MathWorks. *'Interp1' Function*. Accessed: Jul. 13, 2022. [Online]. Available: https://it.mathworks.com/help/MATLAB/ref/interp1.html

[28] *Hocking Phasec 2D, Specification*. Accessed: Jul. 13, 2022. [Online]. Available: http://www.woosungndt.kr/data/phasec2d-data%20sheet.pdf

Alessandro Sardellitti (Graduate Student Member, IEEE) was born in Sora, Italy, in 1993. He received the M.S. degree (*cum laude*) in electrical engineering from the University of Cassino and Southern Lazio, Cassino, Italy, in 2018, where he is currently pursuing the Ph.D. degree in electrical engineering with the Department of Electrical and Information Engineering.

His current research interests concern to the development of methodologies, numerical models, and measurement setup suitable for the realization of nondestructive testing (NDT). On such topic, he has authored or coauthored papers published in international journals and conferences.

Giulia Di Capua (Senior Member, IEEE) received the B.Sc. and M.Sc. degrees (Hons.) in electronic engineering and the Ph.D. degree in information engineering from the University of Salerno, Fisciano, Italy, in 2006, 2009, and 2013, respectively.

From 2013 to 2016 and from 2016 to 2020, she was a Post-Doctoral Researcher and a Research Assistant with the University of Salerno. Since 2021, she has been an Assistant Professor with the Department of Electrical and Informational Engineering, University of Cassino and Southern Lazio, Cassino, Italy. Her research interests include power management, switching-mode power supplies optimization, magnetic components design, and wireless power transfer systems.

Dr. Di Capua is an Associate Editor of the IEEE TRANSACTIONS ON CIRCUITS AND SYSTEMS—I: REGULAR PAPERS (TCAS-I).

Marco Laracca (Member, IEEE) received the M.S. degree in electrical engineering and the Ph.D. degree in electrical and information engineering from the University of Cassino, Cassino, Italy, in 2002 and 2006, respectively.

From 2006 to 2021, he has been an Assistant Professor of electrical and electronic measurements with the University of Cassino. Since 2021, he has been an Associate Professor of electrical and electronic measurements with the Sapienza University of Rome, Rome, Italy. He has been the Chief of the ACCREDIA Notified Metrology Laboratory (LAT 105) since 2018. His current research interests include the realization of the measurement system for nondestructive testing, sensor realization and characterization, electric measurement under nonsinusoidal conditions, and speed calibration.

Antonello Tamburrino (Senior Member, IEEE) received the Laurea degree (*summa cum laude*) in electronic engineering from the University of Naples Federico II, Naples, Italy, in 1992, and the Ph.D. degree in electronic engineering from the Polytechnic University of Turin, Turin, Italy, in 1996.

Since 2006, he has been a Full Professor of electrical engineering with the Department of Electrical and Information Engineering, University of Cassino and Southern Latium, Cassino, Italy. From 2014 to 2018, he was a Full Professor of electrical engineering with the College of Engineering, Michigan State University, East Lansing, MI, USA. He has authored or coauthored more than 250 papers that have appeared in refereed international journals, books, and proceedings of international conferences, and he is a coeditor of three proceedings. His current research interests include inverse problems, electromagnetic imaging, nondestructive evaluation, computational electromagnetism, plasmonics, and homogenization methods.

Salvatore Ventre (Senior Member, IEEE) received the Laurea degree (*summa cum laude*) in electronic engineering from the University of Naples Federico II, Naples, Italy, in 1990.

Since 1993, he has been with the Department of Electrical and Informational Engineering, University of Cassino and Southern Lazio, Cassino, Italy, where he is currently an Associate Professor of electrotechnics. He has authored or coauthored more than 150 technical papers in international journals and conference proceedings. His current research interests include computational electromagnetic with application in several fields, such as electromagnetic nondestructive evaluation, electromagnetic compatibility, analysis of the time evolution of MHD equilibria, and for the identification of the plasma boundary in tokamaks.

Luigi Ferrigno (Senior Member, IEEE) is currently a Full Professor of electric and electronic measurement with the University of Cassino and Southern Lazio, Cassino, Italy. Since 2021, he has been a delegate of the Rector for the technology transfer. Since 2021, he has been an NDE 4.0 Ambassador for the Italian Association of Non-Destructive Evaluation and Test (AiPnD) in the framework of the EFNDT WG10. He has coordinated and participated in several national and international research projects. His current research interests include the NDT4.0 applications, sustainable mobility, novel learning sensors, and measurement systems for smart city and smart energy and applications.

Open Access funding provided by 'Università degli Studi di Roma "La Sapienza"' within the CRUI-CARE Agreement